Isomerization of Pyrrole. Quantum Chemical Calculations and Kinetic Modeling

Faina Dubnikova and Assa Lifshitz*

Department of Physical Chemistry, The Hebrew University of Jerusalem, Jerusalem 91904, Israel

Received: July 31, 1998; In Final Form: October 7, 1998

Density functional theory (DFT) calculations including configuration interaction (CI) were carried out to investigate the pathways of the unimolecular isomerizations of pyrrole. Vibrational frequencies calculated with the DFT method were used to estimate transition-state theory frequency factors. The potentional energy surface of the overall isomerization of pyrrole is composed of pyrrolenine, two biradical intermediates, and five transition states, in addition to pyrrole and its stable isomers. The first step of the isomerization is a fast transition from pyrrole to pyrrolenine. These two species reach a state of equilibrium that is maintained during the entire process. There is no direct path that leads from pyrrole to its stable isomers, which are produced only from pyrrolenine. Two biradical intermediates that are very similar in their structure and energetics and that isomerize to one another by a low-barrier rotation are involved in the process of pyrrole isomerization. One intermediate forms *only cis*-crotonitrile, and the other intermediate forms *only* vinylacetonitrile. These two biradical intermediates and several transition states have resonance structures. There is no direct route that leads from pyrrolenine to *trans*-crotonitrile. The latter is formed from the cis isomer by cis → trans isomerization. RRKM calculations were carried out to transfer values of A_∞ and E_∞ of the rate constants of two high-barrier steps in the isomerizations to A and E corresponding to the experimental conditions. Kinetic modeling, which uses the calculated rate constants, gives a very good agreement between the calculated and the experimental yields of the isomerization products.

1. Introduction

Unimolecular isomerizations and decompositions of five-membered heterocyclic compounds containing oxygen and nitrogen have long been a subject of extensive investigation.[1−6] Whereas decompositions take place whenever such molecules are heated to high temperatures, isomerization reactions do not always take place. The thermal behavior of these molecules depends on the number of double bonds in the ring, on their location, and on the substituents that are attached to the ring. Also, when five-membered ring compounds are fused to the benzene ring, the number of isomerization reactions increases. Thus, furan,[7] dihydrofuran,[8] and tetrahydrofuran[9] do not isomerize, whereas 2,3-dihydrobenzofuran[10] and 1,3-dihydroisobenzofuran[11] isomerize to phenylacetaldehyde and *ortho*-tulylaldehyde, respectively. Isoxazole[12] and 5-methylisoxazole[13] do not isomerize, whereas the isomerization of 3,5-dimethylisoxazole[14] to 2-methyl-3-oxobutironitrile is the main reaction in this molecule. Both in pyrrole[5] and in indole,[6] the main reactions are isomerizations.

The decomposition of pyrrole was studied in the past in this laboratory[5] and by Mackie et al.[1] using the single-pulse shock tube technique. In our study, the temperature range 1050−1450 K was covered, while in Mackie's, the temperature range was 1200−1500 K. At the lower temperature range of our study, three isomerization products, *cis*- and *trans*-crotonitrile ($CH_3CH{=}CHCN$) and vinylacetonitrile ($CH_2{=}CHCH_2CN$) had the highest yield, and only at the high-temperature end of the study the yield of hydrogen cyanide exceeded that of the isomers.[5] This behavior enables one to make a comparison between the experimental results and the calculations regarding the isomerization process. In the higher temperature study, the isomerization products had considerably lower yield than HCN, and at the high-temperature end of the study their yield was lower than those of other decomposition products as well.[1]

Mackie et al.[1] proposed an intermediate species, pyrrolenine (2H-pyrrole), as a precursor to the isomerization products. The pyrrole ⇔ pyrrolenine conversion is a tautomeric reaction in which a hydrogen atom moves from the nitrogen to a neighboring carbon atom. This reaction is much faster than the isomerizations so that pyrrole and pyrrolenine are practically in a state of equilibrium. 1,2 and 1,4 H-atom migrations in pyrrolenine lead to different isomerization products. Whereas the existence of pyrrolenine was never established experimentally (only substituted of pyrrolenines are known[15−17]), quantum chemical calculations can shed light on its function as an intermediate species in the thermal isomerizations of pyrrole. Both Lifshitz et al.[5] and Mackie et al.[1] suggested that only two isomerization products, *cis*-crotonitrile and vinylacetonitrile, are formed in the isomerization of pyrrole and that *trans*-crotonitrile is formed by the cis → trans isomerization of the cis isomer.

We have recently published detailed quantum chemical calculations reporting on the structures and the energetics of the various transition states and intermediates that are involved in the isomerization reactions of cyclopropanecarbonitrile.[18] The latter is an isomer of pyrrole. This compound yields three isomerization products, *cis*- and *trans*-crotonitrile (CRNT) and vinylacetonitrile (VACN). We used the density functional theory (DFT) method and found that the isomerizations proceeded via a biradical mechanism. On the basis of the very good agreement between the DFT and TCSCF (two-configuration self-consistent field) calculations and also between the DFT calculations and experiment, we believe that this method is quite suitable for calculating transition states and intermediates of a biradical nature. This is particularly true when the potential energy surface includes both closed-shell and open-shell singlets. We have thus

10.1021/jp983251r CCC: $15.00 © 1998 American Chemical Society
Published on Web 12/03/1998

used the DFT method also in the present investigation, which deals with quantum chemical and model calculations of the isomerization of pyrrole.

2. Computational Details

In this investigation, we used the Becke three-parameter hybrid method[19] with Lee−Yang−Parr correlation functional approximation[20] (B3LYP) and the Dunning correlation consistent polarized valence double-ξ (cc-pVDZ) basis set.[21,22] (Martin et al.[23] have shown that the use of the triple-ξ basis set (cc-pVTZ) in a line of molecules including pyrrole did not make any improvement that would justify additional computer expense.) Biradical structures were localized using guess wave functions with the destruction $\alpha-\beta$ and spatial symmetries by the unrestricted uB3LYP method. We used an open-shell singlet approximation for the biradical structures. Two biradical structures were also optimized by using of a complete active space multiconfiguration self-consistent field (CASSCF) with CAS(4,4) wave functions for comparison. The reference configuration was defined by filling separately the α and β occupied orbitals (105 singlet configurations). The initial guess wave functions were taken from unrestricted Hartree−Fock (uHF) calculations at optimal uB3LYP geometry.

All the calculations were performed without symmetry restrictions. Vibrational analyses were carried out at the same level of theory to characterize the optimized structures as local minima or transition states. Calculated vibrational frequencies and entropies (at uB3LYP level) were used to evaluate preexponential factors of the reactions under consideration. All the calculated frequencies as well as the zero-point energies are of harmonic oscillators. The calculated frequencies were not scaled since the scaling did not improve the agreement with the experimentally measured frequencies where stable molecules were concerned. The calculations of the intrinsic reaction coordinate (IRC) were done at the uB3LYP level of theory with mass-weighted internal coordinates to check whether the transition states under consideration connect the expected reactants and products. Only this coordinate system permits one to follow the steepest descent path.[24] We computed the IRC path with the same basis set as was used for the stationary point optimization.

Each optimized SCF structure was recalculated at a single-point quadratic CI including single and double substitutions with a triplet contribution to the energy, QCISD(T).[25] QCISD(T) calculations were performed with the frozen core approximation. The DFT and QCISD(T) computations were carried out using the Gaussian-94 program package.[26] The CASSCF(4,4) calculations were carried out using the Gamess-USA program.[27] All calculations were carried out on a DEC Alpha TurboLaser 8200 5/300 at the Institute of Chemistry of The Hebrew University of Jerusalem.

3. Results and Discussion

A. Pyrrole and Pyrrolenine. Table 1 shows selected experimental[28−30] and calculated structural parameters of pyrrole and pyrrolenine (2H-pyrrole) using the B3LYP level of theory with the cc-pVDZ basis set (see Figure 2 for reference to the atom numbering). For pyrrolenine, the calculations are compared to values obtained by X-ray crystal structure measurements of substituted pyrrolenines.[30] As can be seen, the structural parameters of both pyrrole and pyrrolenine are in good agreement with the experimental values. There is slight disagreement between calculations and experiment in the length of the C−C single bond, located between two C═C double bonds in both species. This phenomenon was observed also by Sunderlin et al.,[31] Bachrach,[32] and others.[33−35]

TABLE 1: Experimental and Computed Structural Parameters of Pyrrole and Pyrrolenine at the B3LYP/cc-pVDZ Level of Theory

	pyrrole		pyrrolenine	
parameter[a,b]	computed	exptl	computed	exptl
r-N(1)−C(2)	1.375	1.370,[d] 1.39[e]	1.462	1.46[c]
r-C(2)−C(3)	1.383	1.382, 1.38	1.502	1.50
r-C(3)−C(4)	1.427	1.417, 1.41	1.350	1.35
r-C(4)−C(5)			1.472	1.49
r-N(1)−C(5)			1.293	1.29
∠C(2)N(1)C(5)	109.9	109.8, 109.7	105.7	107.3
∠N(1)C(2)C(3)	107.6	107.7, 107.4	106.9	106.2
∠C(2)C(3)C(4)	107.4	107.4, 108.0	107.0	107.5
∠C(3)C(4)C(5)			106.1	106.2
∠C(4)C(5)N(1)			114.3	112.9
r-H(1)−N(1)	1.010	0.996, 1.01		
r-H(1)−C(2)			1.117	
r-H(2)−C(2)	1.087	1.076, 1.07	1.103	
r-H(3)−C(3)	1.088	1.077, 1.08	1.091	
∠H(1)N(1)C(2)	124.99	125.1		
∠H(1)C(2)N(1)			109.2	
∠H(2)C(2)N(1)	121.16	120.8	110.8	
∠H(2)C(2)C(3)	131.17	130.8	114.7	
∠H(3)C(3)C(2)	125.72	125.5	125.5	
τ-H(1)C(2)C(3)C(4)	0.00		−120.3	
τ-H(2)C(2)C(3)C(4)	180.00		120.1	
τ-N(1)C(5)C(4)C(3)	0.00		0.0	
τ-H(5)C(5)C(4)C(3)	180.00		179.0	

[a] Distances in angstroms, angles in degrees. [b] The atom numbering is shown in Figure 2. [c] Experimental parameters from ref 30. [d] Experimental parameters from ref 28. [e] Experimental parameters from ref 29.

TABLE 2: Experimental[37] and Computed Frequencies (in cm^{-1}) of Pyrrole at the B3LYP/cc-pVDZ Level of Theory and Their Approximate Assignments

	raw		scaled		
exptl[a]	freq	Δ[c] (%)	freq	Δ[c] (%)	approx assignment[d]
474	475	0.2	448	−5.5	N−H out-of-plane
618	629	1.8	593	−4.0	ring deformation
626	642	2.7	606	−3.2	ring deformation
712	686	−3.7	647	−9.1	C−H out-of-plane wag
720	729	1.3	688	−4.5	C−H out-of-plane wag
826	829	0.4	782	−5.3	C−H out-of-plane wag
863	872	1.0	823	−4.7	ring deformation
868	880	1.4	830	−4.4	C−H out-of-plane wag
880	892	1.4	842	−4.4	ring deformation
1018	1027	0.9	969	−4.8	C−C stretch, CCH bend
1049	1058	0.9	998	−4.9	CHH bend
1074	1086	1.1	1025	−4.6	CHH bend
1134	1150	1.4	1085	−4.3	CNH bend, CCH bend
1148	1179	2.7	1112	−3.1	ring breathing
1287	1294	0.5	1221	−5.1	CNH bend, CCH bend
1391	1426	2.5	1345	−3.3	C═C, C−C stretch
1424	1466	2.9	1383	−2.9	C−N stretch
1470	1502	2.2	1417	−3.6	C−N stretch
1521	1576	3.6	1487	−2.2	C═C stretch
3116	3236	3.8	3053	−2.0	C−H stretch
3125	3248	3.9	3064	−1.9	C−H stretch
3140	3264	3.9	3079	−1.9	C−H stretch
3148	3270	3.9	3085	−2.0	C−H stretch
3527	3660	3.8	3453	−2.1	C−N stretch

[a] Gas-phase frequencies from ref 37. [b] Scaling factor is 0.9434.[36] [c] Δ = (calculated value − experimental value)/experimental value, in percent. [d] Mode description from ref 33.

Table 2 shows the B3LYP/cc-pVDZ frequencies of pyrrole both scaled[36] and unscaled. (There are no measured frequencies of pyrrolenine.) As can be seen, the agreement between the calculated and measured frequencies[37] is very good. Scaling the

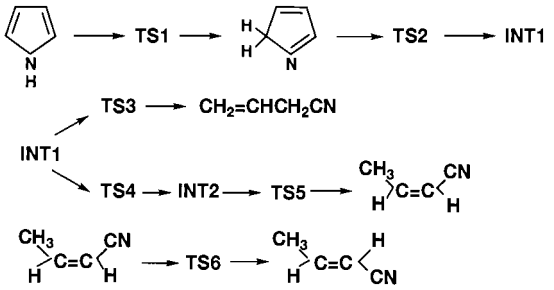

Figure 1. Schematic presentation of the main product formation of pyrrole isomerization.

calculated frequencies does not improve the agreement with the experiment. On the contrary, the percent deviations of the unscaled frequencies are smaller.

B. Structures of the Critical Points along the Pathway of Product Formation. A schematic presentation of the various pathways of the isomerization of pyrrole is shown in Figure 1 and the energetics of the species involved are shown in Table 3 for uB3LYP/cc-pVDZ and uQCISD(T)/cc-pVDZ//uB3LYP/cc-pVDZ. As shown in the scheme, we found that the first stage in this process is the formation of pyrrolenine (2H-pyrrole). IRC analysis indicates that none of the transition states that lead to the intermediates or to the isomerization products are obtained directly from pyrrole. They are obtained only from pyrrolenine.

The existence of pyrrolenine as an intermediate in the isomerization of pyrrole was suggested by Mackie et al.[1] and raised as a possibility in several thermal[38,39] and photochemical[40] rearrangement studies of pyrrole and substituted pyrroles. The pyrrole ⇔ pyrrolenine tautomerism was also a subject of an ab initio investigation,[31,32] where an activation barrier of 44.5 kcal/mol for 1,2 H-atom shift was computed at the MP2/6-31G* level of theory.[32] As can be seen in Table 3, the barrier that we have calculated (pyrrole → TS1) is 44.0 at the B3LYP and 43.1 kcal/mol at the QCISD(T) levels of theory, respectively. The calculated geometrical parameters of the species involved in the isomerization process are shown in Table 4 (except for the parameters of pyrrole and pyrrolenine, which have already been shown in Table 1 in comparison with the experiment) (see Figures 2−6 for the numbering of the atoms). The frequencies, including the imaginary ones, are show in Table 5, and the calculated moments of inertia, entropies, and zero-point energies (ZPE) of pyrrole, pyrrolenine, and all the intermediates and transition states are shown in Table 6. These values were used for calculating Arrhenius parameters for the kinetic modeling.

As can be seen in Figure 2, the reaction coordinate of the transition state TS1, which is a closed-shell transition state, is a 1,2 H-atom shift from the nitrogen atom to an adjacent carbon. The original N−H distance of approximately 1.01 Å in pyrrole stretches to 1.28 Å in TS1, and the new C−H bond that is just about to be formed has a distance of 1.29 Å, practically equal to the N−H distance (Table 4). The two C−N bond lengths, which are exactly the same in pyrrole, 1.375 Å, are very different in the transition state. They are 1.45 and 1.26 Å, pointing to the establishment of a definite C(2)−N(1) single bond and a C(5)−N(1) double bond. All the C−C bond lengths in TS1 have intermediate values between those of pyrrole and pyrrolenine. Whereas the pyrrole and pyrrolenine rings have a planer structure, the planarity of the ring in TS1 is slightly distorted in the area of the H-atom migration. In pyrrolenine, the C(2)−N(1) single bond is longer and weaker than the equivalent bond in pyrrole.

The reaction coordinate of the ring-opening transition state TS2 is a combination of two normal modes, C(2)−N(1) stretch and a rotation of the terminal methylene group H(1)C(2)H(2) with respect to the ring plane. The C(2)−N(1) bond in TS2 is practically ruptured. The C−N distance is 2.48 Å compared to 1.46 Å in pyrrolenine. In addition, all the internal angles CCC and CCN are wider. In contradiction to pyrrole, TS1, and pyrrolenine, the transition state TS2 already has some biradical character, because it is about to form an intermediate INT1, which is a complete biradical (Tables 6 and 7). The structures of TS2 and INT1 are shown in Figure 3. Information on the distribution of atomic spin densities (Table 7), the spin contamination, and the biradical character, χ, (Table 6) enables one to see the differences between the species involved. (χ was calculated using the method of Kraka and Kremer.[41])

The intermediate INT1 is a biradical species with a planar structure. It forms, as can be seen in Figure 1, two species via transition states TS3 and TS4. The reaction coordinate in TS3 is a 1,2 H-atom shift to produce the stable isomer vinylacetonitrile (CH_2═$CH-CH_2CN$). In TS4, it is a rotation of a NCH group with respect to the molecule's plane to produce another intermediate INT2.

As INT1 is a biradical and the nitrogen has an unpaired electron (α-spin) one would have expected that one of the carbon atoms C(2) or C(4) will have the second unpaired electron (β-spin). Such a situation would have resulted in a big difference between the C(2)−C(3) and the C(3)−C(4) bond lengths. The calculations show, however, that these bond lengths (Table 4) and the spin densities on C(2) and C(4) (Table 7) are close to one another. CASSCF(4,4) calculations (which will be described latter) show that they are practically equal. These results suggest a resonance structure similar to what is found in $C_3H_3^{\bullet}$ and other radicals.[42] In fact, this behavior has already been observed in TS2.

Figure 4 shows the reaction path leading from the biradical intermediate INT1 to the stable isomer vinylacetonitrile via the transition state TS3. The reaction coordinate in this path is a 1,2 H-atom shift from C(5) to C(4), which expresses itself by a stretch of the C(5)−H(5) bond from approximately 1.11 to 1.21 Å and a decrease in the distance between C(4) and H(5) from 2.182 Å in INT1 to 1.695 Å in TS3. In addition, the bond distances C(2)−C(3) and C(3)−C(4), which do not differ very much from one another in the intermediate INT1, approach the corresponding distances in vinylacetonitrile, namely, a double bond between C(2) and C(3) and a single bond between C(3) and C(4). The bond distances of the three species that are involved in this path (INT1, TS3, and vinylacetonitrile) are listed in Table 4. As can be seen, TS3, a transition state that connects a biradical with a closed-shell molecule, has only about 20% biradical character (Table 6) and its spin density is also highly delocalized (Table 7).

We tried to locate a transition state that connects the intermediate INT1 to *cis*-crotonitrile (CH_3-CH═$CHCN$), a second stable isomer of pyrrole. The reaction coordinate for this processes is a 1,4 H-atom migration from C(5) to C(2). Despite many trials, this attempt was unsuccessful. As will be shown, the crotonitrile formation takes place from another intermediate, INT2, which is obtained from INT1.

Figure 5 describes the path leading from INT1 to INT2 via TS4. All three species involved in this path are biradicals with $\chi = 1$, for the intermediates, and 0.73, for the transition state. The reaction coordinate in this path is a rotation of the NCH group with respect to the molecule's plane. The plane distortion

TABLE 3: Total Energies E_{total} (in au), Relative Energies ΔE_{total}, and $\Delta E^{\ddagger}$ (in kcal/mol) of All the Critical Points along the Pyrrole Isomerization Profile Calculated at Different Computational Levels[a]

	uB3LYP/cc-pVDZ			uQCISD(T)/cc-pVDZ		
	E_{total}	ΔE_{total}	$\Delta E^{\ddagger}$	E_{total}	ΔE_{total}	$\Delta E^{\ddagger}$
pyrrole	−210.183 015	0.00	0.00	−209.585 592	0.00	0.00
TS1	−210.107 731	47.24	44.01	−209.511 765	46.33	43.10
pyrrolenine	−210.158 367	15.47	14.60	−209.567 785	11.17	10.30
TS2	−210.062 583	75.57	71.13	−209.470 183	72.42	67.98
INT1	−210.071 663	69.87	65.59	−209.474 116	69.95	65.67
INT2	−210.070 825	70.40	66.05	−209.473 052	70.62	66.27
TS3	−210.037 884	91.07	84.44	−209.444 430	88.58	81.95
TS4	−210.061 719	76.11	70.98	−209.466 221	74.91	69.78
TS5	−210.045 400	86.35	79.20	−209.456 275	81.15	74.00

[a] $\Delta E^{\ddagger} = \Delta E_{total} + \Delta(ZPE)$.

TABLE 4: Structural Parameters of Transition States, Intermediates, and Two Products of Pyrrole Isomerizations Calculated at the uB3LYP/cc-pVDZ Level of Theory

parameter[a,b]	TS1	TS2	INT1	INT2	TS3	TS4	TS5	c-CRNT	VACN
r-N(1)−C(2)	1.460	2.478	3.025						
r-C(2)−C(3)	1.409	1.407	1.377	1.380	1.360	1.383	1.454	1.495	1.333
r-C(3)−C(4)	1.399	1.377	1.406	1.405	1.428	1.397	1.353	1.346	1.514
r-C(4)−C(5)	1.403	1.461	1.459	1.454	1.450	1.494	1.472	1.432	1.466
r-N(1)−C(5)	1.356	1.271	1.268	1.268	1.209	1.256	1.228	1.165	1.161
∠C(2)C(3)C(4)	106.5	121.2	126.5	127.5	125.4	126.3	120.0	126.4	126.0
∠C(3)C(4)C(5)	107.5	116.3	126.0	125.2	122.5	124.1	112.8	123.4	114.5
∠C(4)C(5)N(1)	112.5	124.1	128.0	124.7	161.4	116.9	135.8	179.2	179.4
r-N(1)−H(1)	1.280	2.125							
r-H(1)−C(2)	1.294	1.092	1.092	1.092	1.093	1.092	1.094	1.104	1.092
r-H(2)−C(2)	1.090	1.094	1.092	1.091	1.091	1.091	1.096	1.104	1.094
r-H(5)−C(5)	1.090	1.109	1.112	1.110	1.211	1.111	1.194	3.104	2.093
r-H(5)−C(4)			2.182	2.206	1.695				1.105
r-H(5)−C(2)			4.178	2.804			1.877	1.099	
τ-H(1)C(2)C(3)C(4)	−58.1	−153.0	180.0	180.0	177.5	178.4	−136.0	−121.6	180.0
τ-H(2)C(2)C(3)C(4)	162.9	39.9	0.0	0.0	−3.3	3.4	70.0	119.7	0.0
τ-N(1)C(5)C(4)C(3)	3.2	−7.5	0.0	−180.0	−62.9	−81.6	−172.3	179.7	−5.6
τ-H(5)C(5)C(4)C(3)	−174.7	171.2	180.0	0.0	100.2	100.0	5.7	0.0	87.0

[a] Distances in angstroms, angles in degrees. [b] Atom numbering is shown in Figures 2−6.

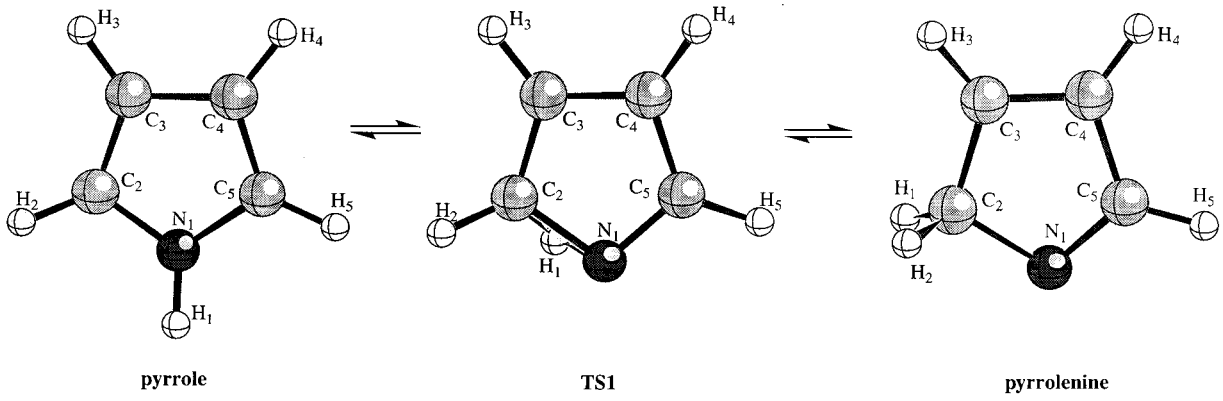

Figure 2. Structure of pyrrole, TS1 and pyrrolenine, the first step of pyrrole isomerization.

in TS4 is 82°, and the net result is a 180° rotation where both INT1 and INT2 are planar (Table 4). Note that the imaginary frequency associated with this reaction coordinate, i-146 cm^{-1}, is very small and compatible with a rotation. All the bond distances in the intermediates INT1 and INT2 are the same. They differ only in the dihedral angles, N(1)C(5)C(4)C(3) and H(5)C(5)C(4)C(3), by 180°. As a result of this rotation, the H(5) hydrogen approaches the C(2) carbon atom, which facilitates a 1,4 H-atom shift from C(5) to C(2) toward the formation of *cis*-crotonitrile.

The formation pathway of *cis*-crotonitrile is shown in Figure 6. This pathway is similar to the INT1 → TS3 → vinylacetonitrile pathway in the sense that in both there is a transition from a biradical species to a closed-shell molecule via a partially biradical transition state (Table 6). There are however significant differences in the details of the reaction coordinates. Whereas the reaction coordinate in the INT1 → TS3 → vinylacetonitrile pathway is simply a 1,2 H-atom shift, the reaction coordinate in the INT2 → TS5 → *cis*-crotonitrile path involves, in addition to a 1,4 H-atom shift from C(5) to C(2), also a considerable movement of C(2) toward the shifting hydrogen. This behavior results also in distortion of the carbon chain in the transition state, which expresses itself by a variation in the CCC angles (Table 4). Note that the imaginary frequency in TS3 is i-1413 cm^{-1} and in TS5 it is i-856 cm^{-1}. The bond distances C(2)−C(3) and C(3)−C(4), which do not differ very much in the

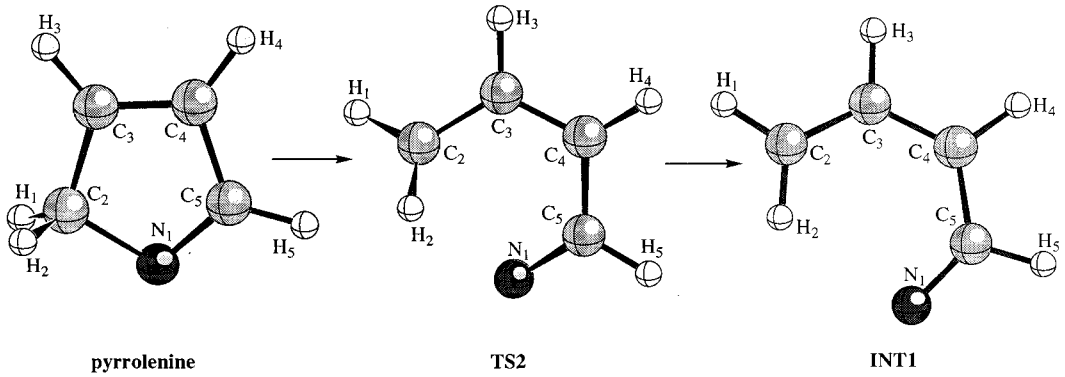

Figure 3. The pathway pyrrolenine → TS2 → INT1, a high-barrier ring-opening process.

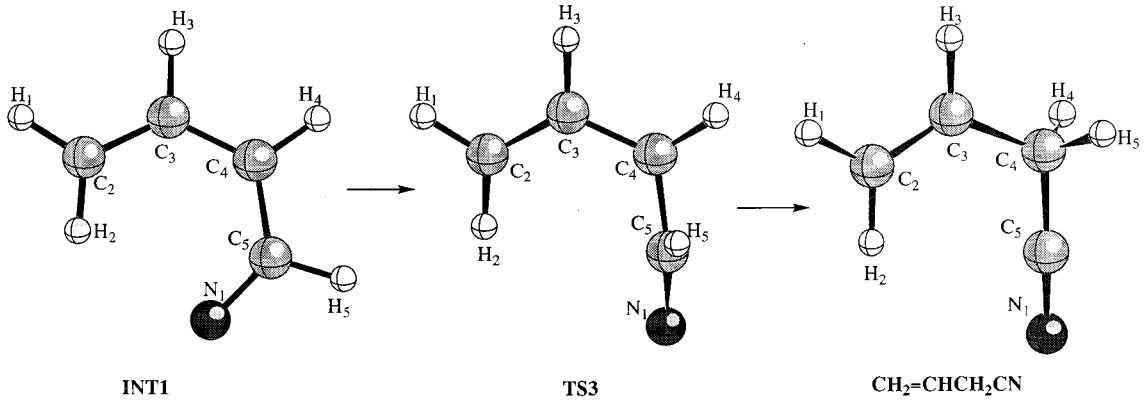

Figure 4. Formation of vinylacetonitrile from the intermediate INT1 via transition state TS3.

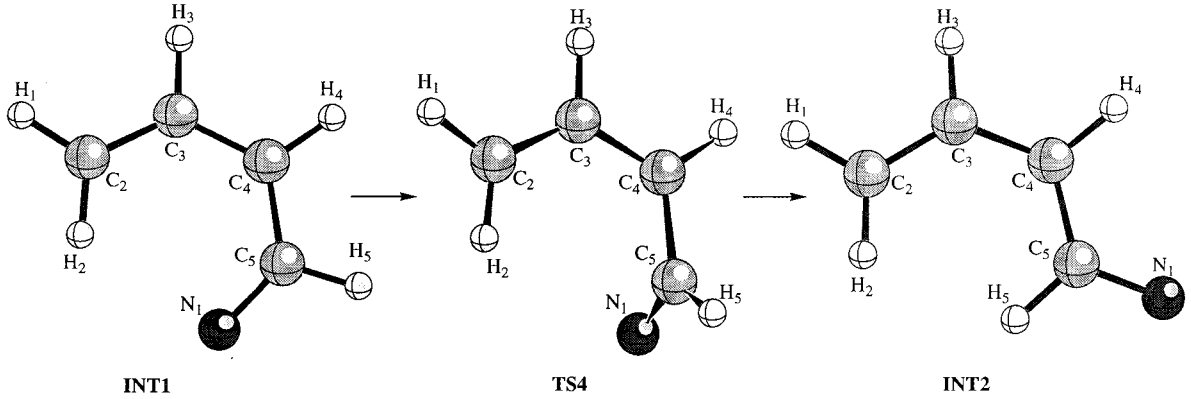

Figure 5. Formation of the intermediate INT2 from INT1 via transition state TS4.

intermediate INT2, approach the corresponding distances of a single bond between C(2) and C(3) and double bond between C(3) and C(4) in *cis*-crotonitrile. The bond distances of the three species involved in this path (INT2, TS5, and *cis*-crotonitrile) are listed in Table 4. The atomic spin densities in the transition state TS5 are high mainly in the vicinity of N(1) and C(2). This finding is in complete accord with a lack of resonance in TS5, namely the existence of distinct single and double bonds in this transition state. This behavior is very different from what has been observed in the other biradicals in this system, where the spin density is high in the vicinity of the nitrogen atom but approximately evenly distributed between C(2) and C(4) (see Table 7 for comparison).

Despite numerous attempts, we could not locate a transition state that leads from INT2 to vinylacetonitrile by a 1,2 H-atom shift. This is somewhat surprising, since INT2 and INT1 have very similar structures so that INT2 could in principle lead also to the formation of a transition state similar to TS3. This issue remains an open question. Also, there is no direct path that leads to the formation of *trans*-crotonitrile from either INT1 or INT2, and, as will be shown later, *trans*-crotonitrile is formed by the cis → trans isomerization of the cis isomer. The details of this process have been recently calculated by the same uB3LYP/cc-pVDZ method.[18]

We have tried to examine the possibility of a reaction path pyrrole → cyclopropanecarbonitrile. The latter is known to isomerize to both *cis*- and *trans*-crotonitrile and vinylacetonitrile. The pyrrole → cyclopropanecarbonitrile isomerization is an endothermic reaction with $\Delta H = 13.4$ kcal/mol. We were unable to locate such a transition state after many trials.

Since we found several species of biradical or partially biradical character having resonance structures along the potential energy surface, we decided to calculate INT1 and INT2 with a multiconfiguration method to see whether the uB3LYP calcula-

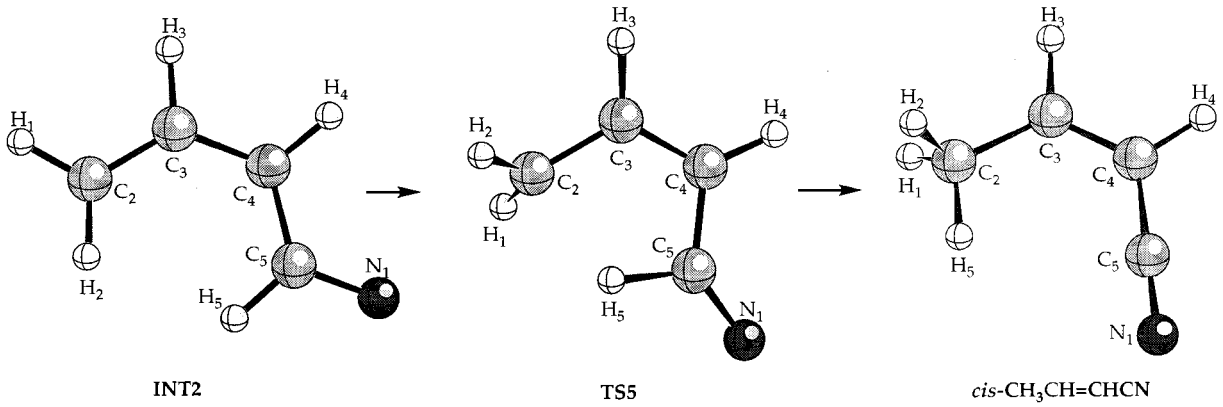

Figure 6. Formation of *cis*-crotonitrile from the intermediate INT2 via transition state TS5.

TABLE 5: uB3LYP/cc-pVDZ Frequencies (cm^{-1}) of the Intermediates and Transition States of Pyrrole Isomerization[a]

TS1	583, 633, 744, 841, 856, 875, 881, 938, 958, 1052, 1073, 1133, 1156, 1241, 1308, 1432, (i-1474), 1484, 1513, 2199, 3212, 3223, 3230, 3248
pyrrolenine	361, 551, 701, 834, 854, 899, 932, 942, 979, 985, 1003, 1105, 1146, 1245, 1302, 1364, 1377, 1551, 1654, 3022, 3051, 3158, 3211, 3234
TS2	297, 418, (i-432), 494, 524, 690, 758, 792, 875, 901, 977, 1013, 1108, 1199, 1212, 1383, 1479, 1495, 1643, 2989, 3137, 3145, 3201, 3238
INT1	143, 226, 333, 399, 546, 672, 722, 872, 879, 916, 994, 1048, 1160, 1232, 1255, 1408, 1425, 1526, 1644, 2948, 3142, 3148, 3187, 3253
INT2	126, 226, 258, 409, 542, 597, 767, 831, 869, 1003, 1004, 1026, 1174, 1202, 1248, 1416, 1442, 1524, 1634, 2979, 3149, 3155, 3196, 3253
TS3	132, 240, 350, 495, 576, 633, 700, 823, 894, 912, 996, 1026, 1140, 1293, 1366, (i-1413), 1425, 1584, 1957, 2130, 3149, 3160, 3203, 3254
TS4	(i-146), 167, 228, 326, 527, 564, 684, 825, 825, 964, 991, 1036, 1147, 1020, 1249, 1394, 1439, 1514, 1713, 2960, 3144, 3153, 3172, 3273, 3258
TS5	204, 289, 462, 530, 625, 691, 756, 850, (i-856), 943, 957, 1005, 1012, 1068, 1154, 1332, 1446, 1596, 1749, 2035, 3119, 3141, 3212, 3220

[a] Imaginary frequencies are shown in parentheses.

TABLE 6: Molecular Parameters of Critical Points in Pyrrole Isomerization

	moments of inertia[a]							
	$A \times 10^{38}$	$B \times 10^{37}$	$C \times 10^{37}$	μ^b	S^c	ZPE[d]	χ^e	$\langle S^2 \rangle^f$
pyrrole	9.2139	0.9362	1.8576	1.99	65.948	51.57		
TS1	9.1964	0.9605	1.8442	1.38	65.188	48.34		
pyrrolenine	9.2642	1.0029	1.8772	1.92	66.111	50.70		
TS2	9.0977	1.4857	2.3518	2.34	68.552	47.13	0.44	0.6939
INT1	8.2143	1.9082	2.7296	2.40	72.617	47.29	1.01	1.0270
INT2	4.8353	2.8936	3.3419	2.95	73.353	47.22	1.01	1.0283
TS3	6.9833	2.3709	3.0127	3.44	72.465	44.94	0.22	0.3914
TS4	7.2928	2.2764	2.7371	2.42	71.759	46.44	0.73	0.9536
TS5	6.1820	2.3507	2.9211	3.51	70.422	44.42	0.38	0.6171

[a] Moments of inertia in g·cm^2. [b] Dipole moments in Debyes. [c] Entropies in cal/(K·mol). [d] Zero-point energies in kcal/mol. [e] Biradical character in % calculated from $\chi = [\Sigma\eta_i - \Sigma\eta_i(\text{ref})]$,[41] where pyrrole was taken as a reference molecule. [f] Spin contamination.

TABLE 7: Atomic Spin Densities of Biradical Species of Pyrrole Isomerization at the uB3LYP/cc-pVDZ Level[a]

	N(1)	C(2)	C(3)	C(4)	C(5)	H(1)	H(2)	H(3)	H(4)	H(5)
TS2	0.63	−0.60	0.18	−0.31	−0.03	0.03	0.03	−0.02	0.02	0.08
INT1	0.70	−0.56	0.21	−0.53	0.00	0.03	0.02	0.00	0.03	0.10
INT2	0.73	−0.60	0.23	−0.52	0.00	0.02	0.03	0.00	0.04	0.09
TS3	0.47	−0.36	0.16	−0.37	−0.12	0.01	0.01	0.00	0.02	−0.18
TS4	0.93	−0.63	0.24	−0.56	−0.12	0.03	0.03	−0.01	0.03	0.07
TS5	0.69	−0.71	0.09	−0.07	−0.16	0.03	0.03	−0.02	0.01	0.13

[a] Positive numbers indicate excess α-spin occupancy, negative numbers excess β-spin occupancy.

tions of these species would be verified. The results obtained by the CASSCF(4,4) did indeed verify the uB3LYP calculations both in energetics and in structure. The bond lengths C(2)−C(3) and C(3)−C(4) in both INT1 and INT2 were very close, indicating a definite resonance structure in the sense that no distinct single or double bonds exist in these intermediates. They were 1.389 and 1.394 Å in INT1 and 1.395 and 1.390 Å in INT2, respectively. In uB3LYP, they were 1.377 and 1.406 Å in INT1 and 1.380 and 1.405 Å in INT2; a structure with single and double bonds would have bond lengths of roughly 1.50 and 1.34 Å, respectively. As can be seen, the existence of the resonance structure is more pronounced in the multiconfiguration calculation. The CASSCF(2,2) calculations of these two intermediates that were first done gave incorrect structures both in

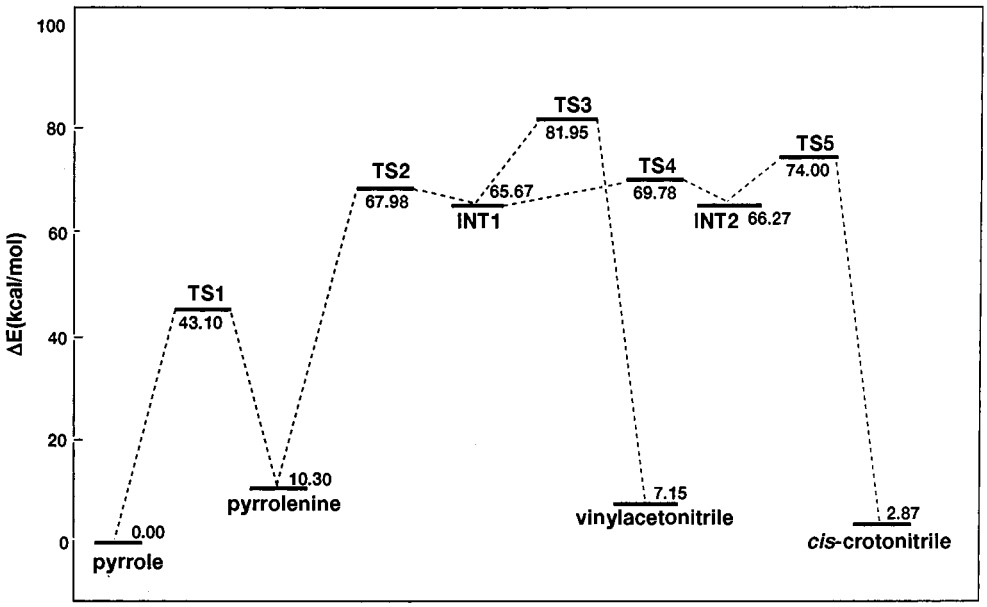

Figure 7. Potential energy profile of pyrrole isomerization. Relative energies $\Delta E^{\ddagger}$ (in kcal/mol) calculated at the uQCISD(T)/cc-pVDZ//uB3LYP/cc-pVDZ level of theory. The energy levels include zero-point energies.

TABLE 8: Reaction Scheme for the Isomerization of Pyrrole

	reaction	σ^a	$\Delta S^{\ddagger\,b}$	$A^{c,d}$/T	$E_a{}^{d,e}$	$A_\infty{}^c$/T	$E_\infty{}^e$	$\Delta S^\circ{}_{\text{reaction}}{}^b$	$\Delta H^\circ{}_{\text{reaction}}{}^e$
1	pyrrole → pyrrolenine	2	−0.76	6.9×10^8	34.6	2.8×10^{10}	43.10	0.16	10.3
2	pyrrolenine → INT1	1	2.44	3.0×10^{10}	55.8	7.1×10^{10}	57.68	6.51	55.4
3	INT1 → VACN	1	−0.15			1.9×10^{10}	16.28	0.28	−58.5
4	INT1 → INT2	1	−0.86			1.4×10^{10}	4.11	0.74	0.6
5	INT2 → *c*-CRNT	1	−2.93			4.8×10^9	8.19	−0.03	−63.4
6	*c*-CRNT → *t*-CRNT	1	2.58	2.1×10^{10}	60.2	8.4×10^{10}	61.09	−0.12	0.1
7	*c*-CRNT → VACN	2	−0.24	4.8×10^{10}	70.6	1.0×10^{11}	70.84	−0.43	4.3
8	*t*-CRNT → VACN	2	−0.03	5.3×10^{10}	71.6	1.1×10^{11}	71.77	−0.31	4.2
2, 3	pyrrolenine → VACN[f]	1	6.35	4.4×10^{11}	71.5	5.1×10^{11}	71.65	6.79	−3.2
2, 4, 5	pyrrolenine → *c*-CRNT[g]	1	4.31	1.2×10^{11}	63.0	1.8×10^{11}	64.16	7.21	−7.4

[a] Reaction coordinate degeneracy. [b] Entropy of activation and entropy of reaction in cal/(K·mol). [c] Preexponential factor in s^{-1}. [d] Activation energy and preexponential factor at 1800 Torr. [e] Activation energy and enthalpy of reaction in kcal/mol. [f] Combines reactions 2 and 3 of the long scheme (see text). [g] Combines reactions 2, 4, and 5 of the long scheme (see text).

terms of bond distances and angles, which indicates that the approximation of the two-configuration self-consistent field is insufficient for this type of calculation.

C. Energetic Characteristics of Pyrrole Isomerization. A schematic diagram of the uQCISD(T)/cc-pVDZ potential energy profile with the relative energy levels of the critical points of pyrrole isomerization is shown in Figure 7. As can be seen, the potential energy surface contains five transition states and two intermediates in addition to the stable molecules. It is of interest to examine the correlation between the various barriers in the profile, the specific reaction coordinates, and the nature of the local minima to which they connect. TS1 is obtained from a closed-shell singlet molecule, pyrrole, and the reaction coordinate is a 1,2 H-atom shift with a barrier of 43 kcal/mol. TS3 has the same reaction coordinate as TS1, but since it is obtained from an unstable biradical, the barrier is much smaller, only 16 kcal/mol. The highest barrier in the profile is that of the ring-opening process, which is found in the transition from pyrrolenine to INT1, 59 kcal/mol. Another interesting comparison is of the transitions INT1 → TS3 and INT2 → TS5. The first transition, which is a 1,2 H-atom shift, is higher in energy by 8 kcal/mol than the second one, which is a 1,4 H-atom shift, with the values being 16 and 8 kcal/mol, respectively. The lowest barrier in the profile, 4 kcal/mol, belongs to the transition from INT1 to INT2, where the reaction coordinate is a simple rotation without changing the skeleton of the molecule. Since the potential energy profile is rather complex, to compare the calculations to the experimental results of the isomerization one must perform computer modeling of all the elementary reactions involved.

4. Comparison with the Experiment

A. Kinetic Modeling. For comparing the calculations with the available experimental results, we have constructed a reaction scheme that contains all steps participating in the isomerization process as well as the interisomerizations among the products taken from a previous investigation.[18] The unimolecular rate constants were calculated from the relation[43,44] $k_\infty = \sigma(kT/h)\exp(\Delta S^{\ddagger}/R)\exp(-\Delta H^{\ddagger}/RT)$, where h is Planck's constant, k is the Boltzmann constant, σ is the degeneracy of the reaction coordinate, and $\Delta H^{\ddagger}$ and $\Delta S^{\ddagger}$ are the enthalpy and entropy of activation, respectively. Values of σ for each reaction are given in Table 8. For isomerization reactions where there is no change in the number of moles $\Delta H^{\ddagger} = \Delta E^{\ddagger}$, where $\Delta E^{\ddagger}$ is the energy difference between the transition state and the reactant. $\Delta E^{\ddagger}$ is equal to $\Delta E^\circ{}_{\text{total}} + \Delta(\text{ZPE})$, where $\Delta E^\circ{}_{\text{total}}$ is obtained by taking the difference between the total energies of the transition state and the reactant and Δ(ZPE) is the difference between the ZPE of these species. Calculated entropies and zero-point energies are shown in Table 6, and total energies and $\Delta E^{\ddagger}$ are in Table 3. To express the rate constants in an Arrhenius

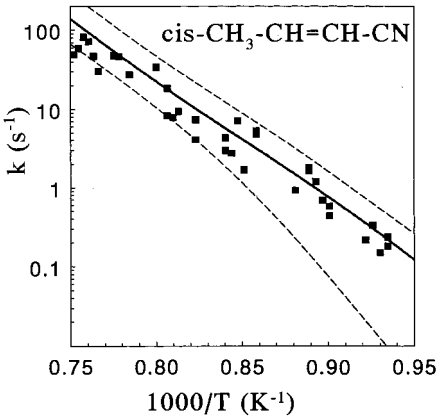

Figure 8. Arrhenius plot of the first-order production rate of *cis*-crotonitrile at 1800 Torr. The squares are experimental points,[5] and the solid line is the best fit through eight calculated points. The upper dashed line shows the results of the computer modeling using the short kinetic scheme (see text). The lower dashed line shows the results of the modeling using Mackie's value for k_1.[1]

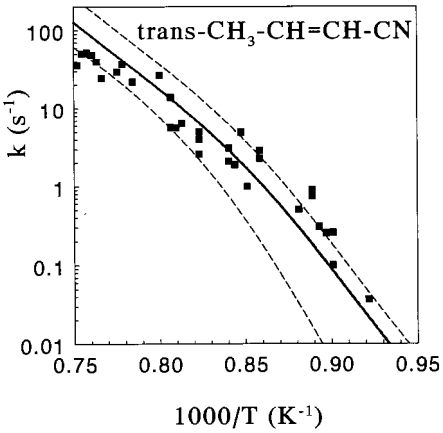

Figure 9. Arrhenius plot of the first-order production rate of *trans*-crotonitrile at 1800 Torr. This product is produced only via cis → trans isomerization of the cis isomer. The squares are experimental points,[5] and the solid line is the best fit through eight calculated points. The upper dashed line shows the results of computer modeling using the short kinetic scheme (see text). The lower dashed line shows the results of modeling using Mackie's value for k_1.[1]

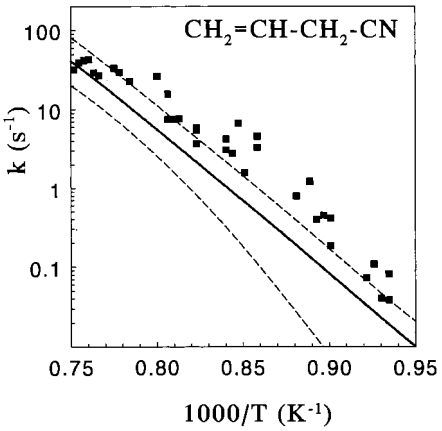

Figure 10. Pyrrole → vinylacetonitrile isomerization at 1800 Torr. The squares are experimental points,[5] and the solid line is the best fit through eight calculated points. The calculated line slightly underpredicts the measured rate. The upper dashed line shows the results of computer modeling using the short kinetic scheme (see text). The lower dashed line shows the results of modeling using Mackie's value for k_1.[1]

form, we replaced $\Delta E^{\ddagger}$ by E_a, where $E_a = \Delta E^{\ddagger} + RT$, and used the relation $k_\infty = \sigma(ekT/h)\exp(\Delta S^{\ddagger}/R)\exp(-E_a/RT)$. A in the expression $k_\infty = A\exp(-E_a/RT)$ is thus given by $A = \sigma(ekT/h)\exp(\Delta S^{\ddagger}/R)$.

We performed RRKM calculations and solved the master equations for two steps that have the highest barriers on the potential energy surface, namely, pyrrole → pyrrolenine and pyrrolenine → INT1. This was done in order to transfer their k_∞ values to the experimental conditions where the data on the isomerizations are available. For steps with low barriers, we used their k_∞ values, as $k(E)$ are so high that the deexcitation is not involved in the process. The RRKM calculations employed a standard routine[45] that uses a direct vibrational state count with classical rotation for the transition state. $\langle\Delta E_{down}\rangle$ was taken as 600 cm^{-1}.[18]

The kinetic scheme containing the reactions that participate in the overall isomerization is shown in Table 8. It contains the high-pressure limit Arrhenius parameters A_∞ and E_∞ and the RRKM calculated parameters for k_1 and k_2 at 1800 Torr. Figure 8 shows the calculated production rate of *cis*-crotonitrile, expressed in terms of a first-order rate constant in the same manner as expressed in the original experimental study.[5] The solid thick line on the figure corresponds to a fit through the points obtained from the modeling calculations done at different temperatures, and the filled squares are the experimental points taken from the article describing the experimental work.[5] Figures 9 and 10 show similar plots of the calculated production rate of *trans*-crotonitrile and vinylacetonitrile, respectively. As can be seen, the calculated production rate of vinylacetonitrile is slightly less than the experimental values, otherwise the agreement is excellent.

Since the pyrrolenine is separated from TS3 and TS5 by a shallow ripple containing the biradicals, from a kinetic viewpoint it is expected that the direct path pyrrolenine → TS3 → vinylacetonitrile and pyrrolenine → TS5 → *cis*-crotonitrile would give about the same results as the reaction scheme containing all the transition states and intermediates. The upper dashed line on each figure shows the results of computer modeling using the kinetic scheme that includes the pyrrole ⇔ pyrrolenine tautomerization, the above-mentioned two paths, and the interisomerization among the reaction products (the short scheme), which is given as part of Table 8. The production rates of the three isomers based on the modeling of the short scheme is somewhat higher but shows a behavior similar to the long scheme. Whereas the existence of the biradical intermediates has no dramatic effect on the chemical kinetic behavior of the system, these intermediates are very significant from the mechanistic viewpoint. The main issue is the fact that INT1 can produce vinylacetonitrile but must undergo low-barrier internal rotation before *cis*-crotonitrile can be formed.

TABLE 9: Sensitivity Spectrum of Pyrrole Isomerization at 1200 K[a]

	reaction	pyrrolenine	*c*-CRNT	t-CRNT	VACN
1	pyrrole → pyrrolenine	0	0	−1	0
2	pyrrolenine → INT1	2	−90	−90	−90
3	INT1 → VACN	0	1	1	−98
4	INT1 → INT2	1	−85	−85	8
5	INT2 → *c*-CRNT	2	−98	−98	9
6	*c*-CRNT → *t*-CRNT	0	54	−97	0
7	*c*-CRNT → VACN	0	0	0	0
8	*t*-CRNT → VACN	0	0	0	0

[a] Percent change in product yields due to a 100-fold decrease in *k*.

B. Sensitivity Analysis. Table 9 shows the sensitivity spectrum of the reaction scheme. The table gives the percent change in the yield of a given product at a reaction time of 2

ms at 1200 K due to a 10-fold decrease in the rate constant of each reaction. An interesting feature in the spectrum is the lack of influence of reaction 1 on the yield of pyrrolenine and on the yield of all the other products, although this reaction forms the pyrrolenine from which all the products are obtained. The reason, as can be seen from the modeling calculations, is that the pyrrole and pyrrolenine are at equilibrium as of the very early stages of the reaction. This is still true even if k_1 and k_{-1} are decreased by a factor of 10. Mackie et al.[1] used a rate constant for reaction 1 of $k_1 = 10^{12} \exp((-58.0 \times 10^3)/RT)$ s^{-1}, lower than our calculated value at 1200 K by a factor of about 1.5×10^4. The lower dashed lines in Figures 8−10 show the results of the modeling using Mackie's value for k_1. With this k_1, reaction 1 begins to affect the overall rate of the isomerization, as can be seen from Figures 8−10. Sensitivity analysis of a scheme using Mackie's value for k_1 shows a very strong effect of k_1. We believe that Mackie's value for the reaction barrier of the pyrrole → pyrrolenine reaction is overestimated, although at his temperatures the affect of his k_1 on the overall isomerization is very small.

In general, the sensitivity spectrum of the isomerization is self-explanatory. The pyrrolenine → INT1 step (reaction 2) has a very strong effect on all the isomers, as this is a high-barrier reaction that precedes all the isomerization steps. Reactions 3 and 5 have exactly the same rate, indicating that the INT1 → INT2 isomerization determines the production rate of *cis*-crotonitrile, whereas reaction 4, which is about 10 times slower than reactions 3 and 5, does not disturb the interrelation between reactions 3 and 5. Interisomerization between vinylacetonitrile and crotonitrile has no effect on the system.

5. Conclusions

The isomerization of pyrrole can be summarized by the following features:

(1) The first step of the isomerization is a fast transition from pyrrole to pyrrolenine. These two species reach, at the very early stages of reaction, a state of equilibrium that is maintain during the entire process.

(2) There is no direct path from pyrrole to its stable isomers; isomerization proceeds via pyrrolenine.

(3) Two biradical intermediates that are related to one another by rotation and that are very similar in their structures and energetics are involved in the isomerization process. One forms *only cis*-crotonitrile, and the other forms *only* vinylacetonitrile. These two biradical intermediates and several of the transition states have a definite resonance structure. The transition state TS5 connecting INT2 to *cis*-crotonitrile has no resonance structure.

(4) There is no direct route leading from pyrrolenine to *trans*-crotonitrile. The latter is formed from the cis isomer by cis → trans isomerization.

(5) Kinetic modeling using the calculated rate constants gives good agreement between the calculated and the experimental yields of the isomerization products.

Acknowledgment. The authors thank the Ministry of Absorption for a fellowship to F.D.

References and Notes

(1) Mackie, J. C. *Int. J. Chem. Kinet.* **1991**, *23*, 733.
(2) Bruinsma, O. S. L.; Tromp, P. J. J.; de Sauvage Nolting, H. J. J.; Moulijn, J. A. *Fuel* **1988**, *67*, 334.
(3) Grela, M. A.; Amorebieta, V. T.; Colussi, A. J. *J. Phys. Chem.* **1985**, *89*, 38.
(4) Lifshitz, A.; Tamburu, C.; Shashua, R. *J. Phys. Chem.* **1997**, *101*, 1018.
(5) Lifshitz, A.; Tamburu, C.; Suslensky A. *J. Phys. Chem.* **1989**, *93*, *5802*.
(6) Laskin, A.; Lifshitz, A. *J. Phys. Chem.* **1997**, *101*, 7787.
(7) Lifshitz, A.; Bidani, M.; Bidani, S. *J. Phys. Chem.* **1986**, *90*, 5373.
(8) Lifshitz, A.; Bidani, M.; Bidani, S. *J. Phys. Chem.* **1986**, *90*, 6011.
(9) Lifshitz, A.; Bidani, M.; Bidani, S. *J. Phys. Chem.* **1986**, *90*, 3422.
(10) Thermal reactions of 2,3-dihydrobensofuran. Unpublished results.
(11) Thermal reactions of 1,3-dihydro isobensofuran. Unpublished results.
(12) Lifshitz, A.; Wohlfeiler, D. *J. Phys. Chem.* **1992**, *96*, 4505.
(13) Lifshitz, A.; Wohlfeiler, D. *J. Phys. Chem.* **1992**, *96*, 7367.
(14) Lifshitz, A.; Tamburu, C.; Wohlfeiler, D. *J. Phys. Chem.* **1995**, *99*, 11436.
(15) Sammes, M. P.; Katritsky, A. R. *Adv. Heterocycl. Chem.* **1982**, *32*, 233.
(16) Laurent, A.; Mison, P.; Nafti, A.; Pellisier, N. *Tetrahedron Lett.* **1982**, *23*, 655.
(17) Sammes, M. P.; Chung, M. W. L.; Katritzky, A. R. *J. Chem. Soc., Perkin Trans. 1* **1985**, 1773.
(18) Dubnikova, F.; Lifshitz, A. *J. Phys. Chem.* **1998**, *102*, 5876.
(19) Becke, A. D. *J. Phys. Chem.* **1993**, *98*, 5648.
(20) Lee, C.; Yang, W.; Parr, R. G. *Phys. Rev.* **1988**, *B37*, 785.
(21) Dunning, T. H., Jr. *J. Phys. Chem* **1989**, *90*, 107.
(22) Kendall, R. A.; Dunning, T. H., Jr.; Harrison, R. J. *J. Phys. Chem.* **1992**, *96*, 6796.
(23) Martin, J. M. L.; El-Yazal, J.; Francois, J. P. *Mol. Phys.* **1995**, *86*, 1437.
(24) Shaik, S. S.; Schlegel, H. B.; Walfe, S. *Theoretical Aspects of Physical Organic Chemistry the SN2 Mechanism*; Wiley: New York, 1992; p 45.
(25) Pople, J. A.; Head-Gordon, M.; Raghavachari, K. *J. Chem. Phys.* **1987**, *87*, 5968.
(26) Frisch, M. J.; Trucks, G. W.; Schlegel, H. B.; Gill, P. M. W.; Johnson, B. G.; Robb, M. A.; Cheeseman, J. R.; Keith, T.; Petersson, G. A.; Montgomery, J. A.; Rahavachari, K.; Al-Laham, M. A.; Zakrzewski, V. G.; Orviz, J. V.; Foresman, J. B.; Cioslowski, J.; Stefanov, B. B.; Nanayakkara, A.; Challacombe, M.; Peng, C. Y.; Ayala, P. Y.; Chen, W.; Wong, M. W.; Andres, J. L.; Replogle, E. S.; Gomperts, R.; Martin, R. L.; Fox, D. J.; Binkley, J. S.; Defrees, D. J.; Baker, J.; Stewart, J. P.; Head-Gordon, M.; Gonzalez, C., Pople, J. A. *GAUSSIAN 94*, revision D.4; Gaussian, Inc.: Pittsburgh, 1995.
(27) Schmidt M. W.; Baldridge, K. K.; Boatz, J. A.; Elbert, S. T.; Gordon, M. S.; Jensen, J. H.; Koseki, S.; Matsunaga, N.; Nguyen, K. A.; Su, S. J.; Windus, T. L.; Dupuis, M.; Montgomery, J. A. *GAMESS-USA*, revision Mar., 1997. See, for example: Schmidt M. W.; Baldridge, K. K.; Boatz, J. A.; Elbert, S. T.; Gordon, M. S.; Jensen, J. H.; Koseki, S.; Matsunaga, N.; Nguyen, K. A.; Su, S. J.; Windus, T. L.; Dupuis, M.; Montgomery, J. A. *J. Comput. Chem.* **1993**, *14*, 1347.
(28) Nygaard, L.; Nielsen, J. T.; Kirchheiner, J.; Maltesen, G.; Rastrup-Andersen, J.; Soerensen, G. O. *J. Mol. Struct.* **1969**, *3*, 491.
(29) Bernardi, F.; Bottoni, A.; Venturini, A. *J. Mol. Struct. (THEOCHEM)* **1988**, *163*, 173.
(30) Gambacorta, A.; Nicoletti, R.; Cerrini, S.; Fedeli, W.; Gavusso, E. *Tetrahedron Lett.* **1978**, 2439.
(31) Sunderlin, L. S.; Panu, D.; Puranik, D. B.; Ashe, A. J., III; Squires, R. R. *Organometallics* **1994**, *13*, 4732−4740.
(32) Bachrach, S. M. *J. Org. Chem.* **1993**, *58*, 5414.
(33) Kofranek, M.; Kovar, T.; Karpfen, A.; Lischka, H. *J. Chem. Phys.* **1992**, *96*, 4464.
(34) Nagy, P. I.; Durant, G. J.; Smith, D. A. *J. Am. Chem. Soc.* **1993**, *115*, 2912.
(35) Hinchliffe, A.; Soscun, M. H. J. *J. Mol. Struct. (THEOCHEM)* **1995**, *331*, 109.
(36) Wong, M. W. *Chem. Phys. Lett.* **1996**, *256*, 391.
(37) Navarro, R.; Orza, J. M. *An. Quim.* **1983**, *A79*, 557.
(38) Jacobson, I. A.; Jensen, H. B. *J. Phys. Chem.* **1962**, *66*, 1245.
(39) Jacobson, I. A.; Jensen, H. B. *J. Phys. Chem.* **1964**, *68*, 3068.
(40) Rendal, W. A.; Torres, M.; Lown, E. M.; Strausz, O. P. *Rev. Chem. Intermed.* **1986**, *6*, 335.
(41) Kraka, E.; Cremer, D. *Chem. Phys. Lett.* **1993**, *216*, 333.
(42) Boyd, S. L.; Boyd R. J.; Barclay L. R. C. *J. Am. Chem. Soc.* **1990**, *112*, 5724.
(43) Eyring, H. *J. Chem. Phys.* **1935**, *3*, 107.
(44) Evans, M. G.; Polanyi, M. *Trans. Faraday Soc.* **1935**, *31*, 875.
(45) Kiefer, J. H.; Shah, J. N. *J. Phys. Chem.* **1987**, *91*, 3024.